Fibers and Polymers 2014, Vol.15, No.4, 753-761 DOI 10.1007/s12221-014-0753-3

Optimization of a Profile Extrusion Die for Flow Balance

Oktay Yilmaz*, Hasan Gunes, and Kadir Kirkkopru

Faculty of Mechanical Engineering, Department of Mechanical Engineering, Istanbul Technical University, Istanbul 34437, Turkey

(Received July 8, 2013; Revised September 4, 2013; Accepted September 12, 2013)

Abstract: One of the problems encountered in the extrusion of plastic profiles is unbalanced flow at the die exit. It causes deformation of the extrudates at ambient and precludes the material transition through remaining stages of production process (calibration, cooling sections etc). In this paper, geometric parameters of a profile extrusion die are optimized using several objective function definitions by Simulated Annealing-Kriging Meta-Algorithm. Objective functions are defined based on the uniformity of velocity distribution at the die exit. For this, Computational Fluid Dynamics (CFD) simulations are performed for N=70 die geometries. Appropriate geometric parameters (t and L) of the die are variables for the optimization problem.

Keywords: Polymer extrusion, Optimization, Objective function, CFD

Introduction

A wide variety of products are produced by polymer extrusion in plastics industry such as pipes, tubes, cable coatings, films, sheets and bottles. Profiles are an essential group of these products. Mainly, two problems exist in the manufacturing process of plastic profiles. These are die swell and flow balance at the die exit. Die swell is fundamentally related to viscoelastic properties of plastics. On the other hand, flow balance is related to die channel geometry feeding die exit section. Unbalanced flow at the die exit causes deformation of extrudate profile. Several researchers studied the flow balance problem in profile extrusion [1-15]. In early studies, profile cross section of extrusion dies was divided into several specific subsections such as circular, slit or annular, and analytical expressions between pressure drop and flow rate were used in order to balance the flow at the die exit [14,16]. However, profile extrusion dies designed with this technique still need revisions in order to reach optimum die geometry in terms of flow balancing. Hence, recently analytical expressions are used for determination of initial dimensions of profile extrusion dies [11]. The cross-section method [17,18] was used for the optimization of profile extrusion dies by several researchers [1,13,14] in order to avoid 3D Computational Fluid Dynamics (CFD) computations. In the cross-section method, 2D slices perpendicular to the die axis are chosen through the profile die and the velocity distribution is computed for fully developed flow conditions for each die slices. Recently, the cross section method is applied successfully for the optimization of uPVC profile dies [13].

Hurez and Tanguy [1] used analytical expressions and the cross-section method for the optimization of a profile die by changing the lengths of the die land channels by trial and error method. After early studies, currently 3D CFD simulations together with optimization techniques are used to accelerate a successful profile die design. Kaul and Michaeli [3] divided the flow domain into finite volumes and determined the flow resistance of each finite volume by CFD simulation. Then, the flow network approach coupled with the evaluation strategy for optimization is employed. Nobrega *et al.* [6] used Finite Volume Method (FVM) for 3D CFD simulations with Simplex Method as optimization algorithm for the design of a profile extrusion die. Sun and Gupta [8] optimized the geometric parameters of a coat-hanger die employing Broyden-Fletcher-Goldfarb-Shanno (BFGS) optimization algorithm by Finite Element Method (FEM) simulations. Shahreza *et al.* [11] performed several CFD simulations of a profile die for different values of design parameters and used Newton's Method for minimization of an introduced objective function. Ettinger *et al.* [13] employed the cross-section method coupled with BFGS and Fletcher-Reeves (FR) optimization method for profile die design.

Several techniques are used within above optimization methods to obtain uniform velocity distribution at the profile extrusion die exit [7,19]. These techniques are related to the optimization of the die land length [1,2,6,11] and channel thicknesses [6]. In addition to these techniques, flow separators are used to obtain balanced flow at the die exit by preventing cross flows [2,14]. However, flow separator may have negative effect on the mechanical properties of the produced profile due to possible welding lines at the interface of the sub-sections [6,7] and sensitivity of profile dies with flow separators to changes in process conditions increases in terms of flow balance. Restrictors are also employed for flow balancing in order to compensate changes in process material rheology and changes in process conditions [9,10]. Pittman [19] in his review paper discussed various aspects of profile die design and optimization.

In the present study, geometric parameters of a profile extrusion die are optimized using different objective function definitions by Simulated Annealing-Kriging Meta-Algorithm

*Corresponding author: yilmazo@itu.edu.tr

[20,22] aided by 3D FEM simulations. The optimization algorithm employed in the current study does not need an analytical objective function for the flow balance parameters. Length and channel thickness optimization for the profile die is performed without using flow separators.

Optimization Problem

An L-shaped extrusion die in Figure 1 which was studied on before [20] is optimized for flow balance based on a suitable objective function (OF) selected from several OF definitions.

The difference between the thicknesses of the horizontal channel (ES1) and the vertical channel (ES2) in Figure 1 results in a non-homogeneous velocity distribution at the die exit. Hence, it is aimed to decrease the flow resistance of the horizontal channel with the introduction of a thick channel as depicted in Figure 2. The optimization variables for the profile die are the thickness of the thick channel t and the length of the narrow channel L as shown in Figure 2. Transition angle α from thick channel to narrow one is fixed at a constant value in order to avoid the length of the transition zone to be an affecting factor on flow balance at the die exit.

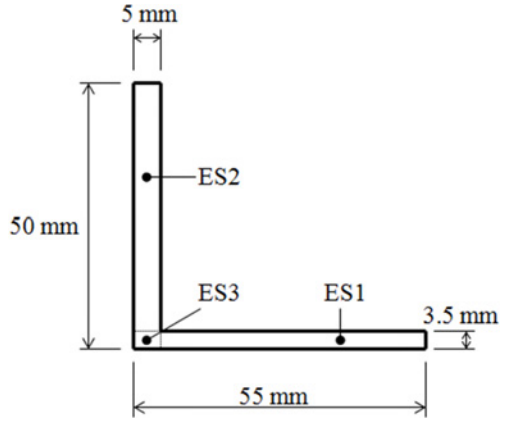

Figure 1. The L-shaped profile.

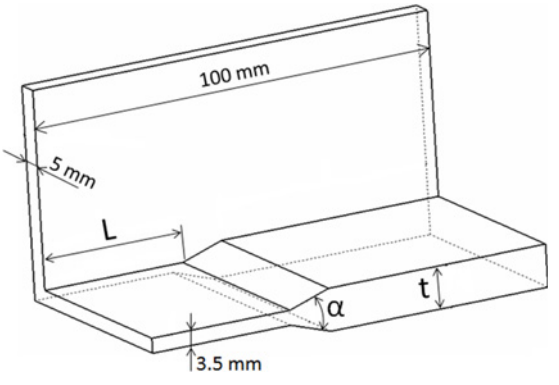

Figure 2. The introduction of a thick channel for the L-shaped profile.

Table 1. Design variables and constraints for the profile die

Design variables	α (deg)	L (mm)	t (mm)
Constraints	30 (fixed)	$15 \le L \le 60$	$5 \le t \le 15$

Therefore, proposed maximum transition angle α=30 ^{o} for avoiding excessive elastic deformations of polymer molecules [16] is selected in this study. The constraints for the design variables (t and L) are shown in Table 1.

The die balance is based on the deviation of the velocity with respect to the average velocity at the die exit or in other words production rate. A definite scale factor between extrudate just exiting the die and final product always exists. Several OFs are used and tested for the optimization problem.

Optimization Process

To start with, Latin Hypercube Sampling (LHS) [21] is employed for the determination of N die geometries (t_i, L_i, i=1 to 70) which are used in the optimization algorithm together with the corresponding OF values. LHS gives randomly distributed design points in t-L parameter space satisfying the constraints in Table 1. Thereafter, N=70 die geometries are created and meshed in Gambit meshing software. The velocity distributions at the die exit for these dies are obtained by means of CFD simulations conducted on PolyFlow software [23] which uses the finite element method and is employed for the simulation of non-newtonian fluid flows [12,19]. The OF values are calculated based on the velocity distribution at the die exit. Finally, N=70 design points and the corresponding OF values are submitted to the Simulated Annealing-Kriging Meta-Algorithm [20,22] developed in Matlab and the optimization algorithm reaches the optimum design point (t^*, L^*).

The optimization algorithm consists of two stages. At the first stage, the Kriging model [22] is constructed based on the number of N design points and the corresponding OF values in order to estimate unknown OF values interpolating the known data in t-L parameter space. Kriging is an estimation technique invented by Krige [24]. French engineer Prof. Georges Matheron formalized Krige's empirical work for evaluation of mineral resources in the 1960s [25].

At the second stage of the optimization algorithm, Simulated Annealing (SA) in conjuction with Kriging Interpolation is employed. SA Method which is invented by Kirkpatrick *et al.* [26] is a generic probabilistic meta-algorithm for global optimization. During iterations in SA algorithm, if new solution is better than the old one, the old solution (current solution) is replaced by a random nearby solution (new solution). In the opposite case, the optimization algorithm acts according to the value of the probability function which is a function of the difference between the new and the old solutions and a global parameter called temperature T for determination on moving to new design point (t_{new}, L_{new}) or

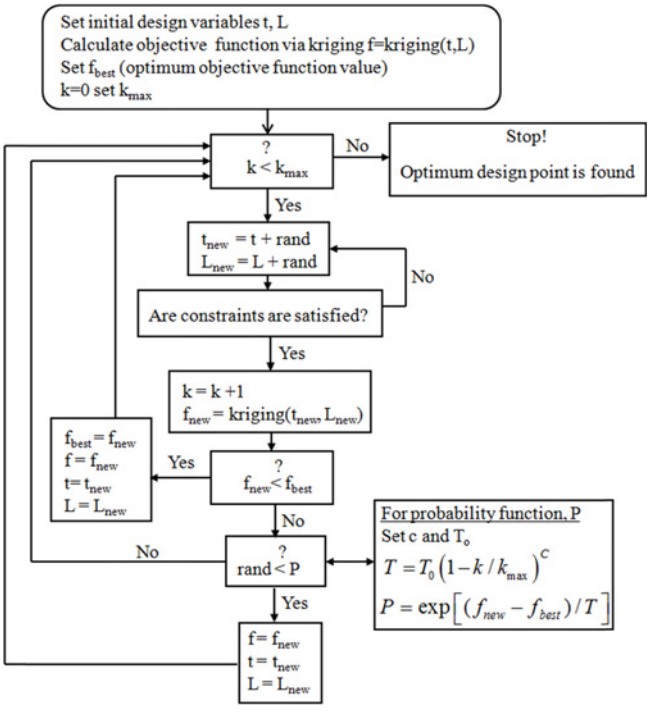

Figure 3. Flow chart of the optimization process [20].

searching another design point around the old one. This structure of the SA algorithm allows uphill moves of the current solution and prevents to become trapped at local minimum points [20,22]. Flow chart of the optimization algorithm Simulated Annealing-Kriging Meta-Algorithm is given in Figure 3.

Computational Fluid Dynamics Simulations

CFD simulations are performed for incompressible, laminar flow of polymer melt through the L-shaped die in isothermal conditions considering that die temperature is controlled at a fixed value. Due to very high viscosity of the polymer melt, inertial and gravitational forces are negligible and this yields a balance between viscous and pressure forces. The governing equations of the polymer flow for the current study are given as follows:

$$\frac{\partial v_i}{\partial x_i} = 0 \tag{1}$$

$$\frac{\partial p}{\partial x_i} = \frac{\partial \tau_{ij}}{\partial x_j} \tag{2}$$

Viscous terms in equation (2) are modeled by Generalized Newtonian Fluid (GNF) Model [27].

$$\tau_{ij} = \eta(\dot{\gamma})\dot{\gamma}_{ij} \tag{3}$$

Here, $\eta(\dot{\gamma})$ is the viscosity function of the polymer melt and $\dot{\gamma}_{ij}$ is the strain-rate tensor.

Table 2. The coefficients of the viscosity model for the polymer melt at 170 °C [28]

η_0 (Pa.s)	λ (s)	n (-)
8920	1.58	0.496

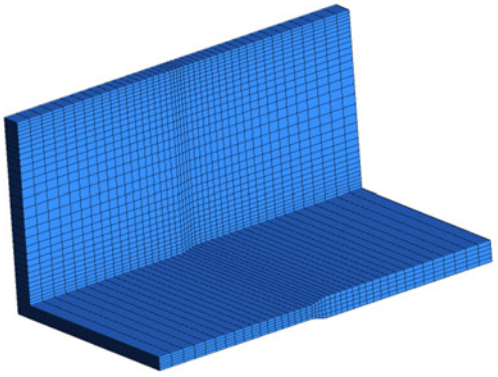

Figure 4. Computational mesh of a die from N=70 die geometries.

A high density polyethylene (HDPE) is extruded through the L-shaped extrusion die in CFD simulations. The Bird-Carreau Viscosity Model (equation (4)) parameters of this material are given in Table 2.

$$\eta(\dot{\gamma}) = \eta_0[1 + (\lambda\dot{\gamma})^2]^{(1-n)/2} \tag{4}$$

Here, η_0, λ and n are zero-shear-viscosity, relaxation time and power-law index of HDPE, respectively.

The following boundary conditions are applied in numerical simulations. The flow is fully-developed at the inlet. No-slip boundary conditions are applied at the die walls. Normal stresses and tangential velocities are zero at the die exit plane. Average velocity at the die exit (or production rate) is 20 m/min. Computational mesh of a die from N=70 die geometries is depicted in Figure 4. The unbalanced flow at the exit of the non-optimized die is clearly seen in Figure 14(a) as a result of post processing of performed CFD simulation.

Objective Function Selection

Some OF definitions introduced in the literature are employed in this section. For this aim, the die exit plane is divided into 3 elemental sections (ESs) as shown in Figure 1. ES1 and ES2 in Figure 1 are considered at first in order to define an OF, since these sections form the main parts of the profile.

$$f_{obj\_1} = \sqrt{\frac{1}{2}[(v_1 - v_{ave})^2 + (v_2 - v_{ave})^2]} \tag{5}$$

This function was employed before for the optimization of profile extrusion dies [2,9]. Here, v_1 and v_2 are the average velocities at ES1 and ES2. v_{ave} is the mean velocity at the die

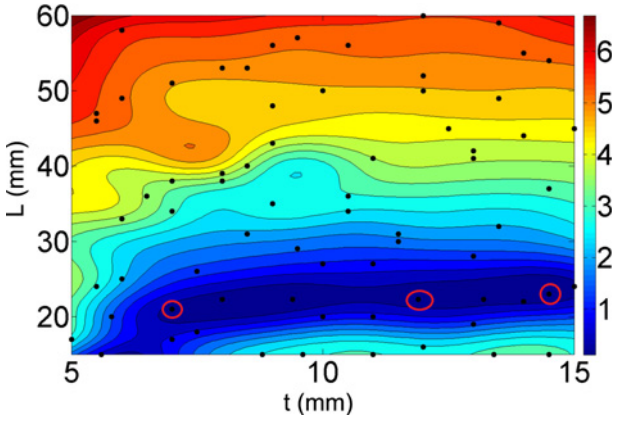

Figure 5. The contours of the objective function (f_{obj_1}) calculated by Kriging model (black points are LHS points).

Table 3. The average velocities at each ES and values of objective function (f_{obj_1})

	t (mm)	L (mm)	v_1 (m/min)	v_2 (m/min)	v_3 (m/min)	f_{obj_1} (m/min)
Die 0	(no modification)		9.92	27.61	19.86	8.93
Die 1	7	21	19.50	20.18	22.75	0.37
Die 2	11.9	22	20.11	19.59	24.42	0.30
Die 3	14.5	23	19.83	19.80	24.47	0.19

exit plane or production rate which is aimed to be 20 m/min. The contours of f_{obj_1} are given in Figure 5. Black points in Figure 5 are LHS points which are used in Kriging Interpolation in order to obtain contours of OF in t-L parameter space. Optimum design points are located in the darkest blue area according to the contours of f_{obj_1} as seen in Figure 5. Optimum design points have almost the same values of L, but t can have values in a large interval. Therefore, three design points having different values of t through that interval in Figure 5 are selected for detailed analysis of flow balance at the die exit.

The OF values for the three dies and the mean velocity values at each ES are given in Table 3. Though, v_1 and v_2 are close to the mean velocity 20 m/min for all dies, v_3 is relatively large for the Die 2 and Die 3. The velocity profiles along the center lines of the vertical channel exit plane and horizontal channel exit plane are shown in Figure 6 for these three dies. The velocity profile at the vertical channel is more uniform for the Die 1 which has the lowest t in Figure 6. Those results show that f_{obj_1} misleads about optimum design point. Hence, v_3 is inserted into a new OF in order to obtain more uniform velocity profile at the vertical channel exit plane for the optimum die geometry.

Introduced second OF [6,12,13] is as follows.

$$f_{obj\_2} = \sqrt{\varphi_1[(v_1 - v_{ave})^2 + \varphi_2(v_2 - v_{ave})^2 + \varphi_3(v_3 - v_{ave})^2]} \quad (6)$$

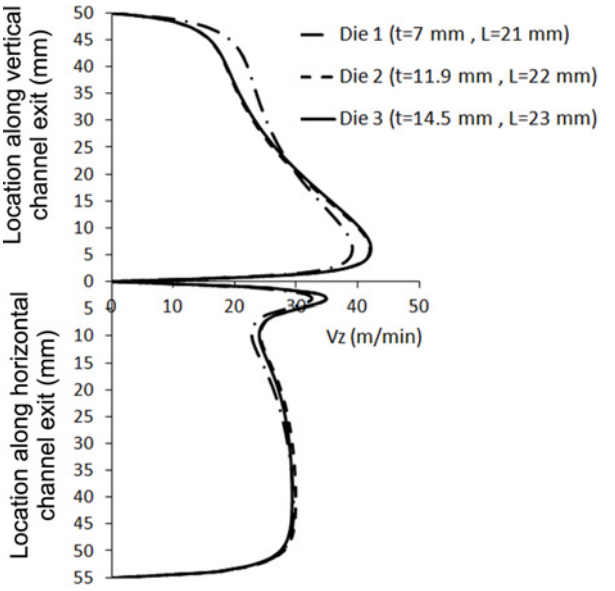

Figure 6. Velocity profiles along the center lines of the vertical channel exit plane (ES2 and ES3) and horizontal channel exit plane (ES1 and ES3).

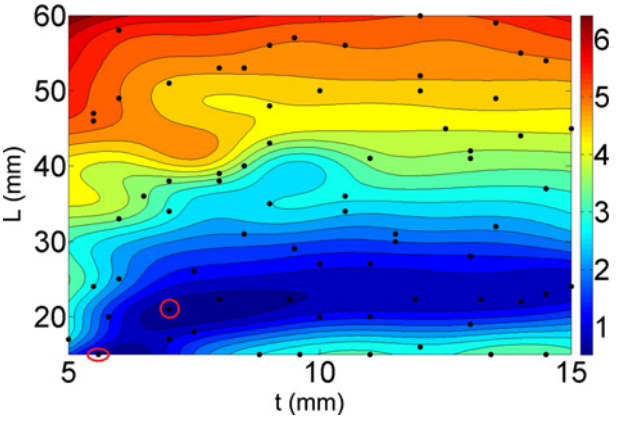

Figure 7. The contours of the objective function (f_{obj_2}) calculated by Kriging model (black points are LHS points).

Here φ_1, φ_2 and φ_3 are area-weighted constants of each ES and their values are 0.41, 0.55 and 0.04, respectively. These constants are the ratio of each ES's area and total die exit plane area. The contours of f_{obj_2} are given in Figure 7. Optimum design points are located in the two darkest blue areas as seen in Figure 7. In order to analyze the suitability of f_{obj_2}, one design point from each of the two optimum regions in t-L parameter space is chosen as shown in Figure 7. The OF values for the two dies and the mean velocity values at each ES are given in Table 4. The velocity profiles along the center lines of the vertical channel exit plane and horizontal channel exit plane are depicted in Figure 8 for the two dies. The velocity v_3 for the Die 4 is lower than one for the Die 1 and velocity distribution at the vertical channel exit

Table 4. The average velocities at each ES and values of objective function (f_{obj_2})

	t (mm)	L (mm)	v_1 (m/min)	v_2 (m/min)	v_3 (m/min)	f_{obj_2} (m/min)
Die 0	(no modification)		9.92	27.61	19.86	8.58
Die 1	7	21	19.50	20.18	22.75	0.65
Die 4	5.6	15	19.10	20.55	21.81	0.80

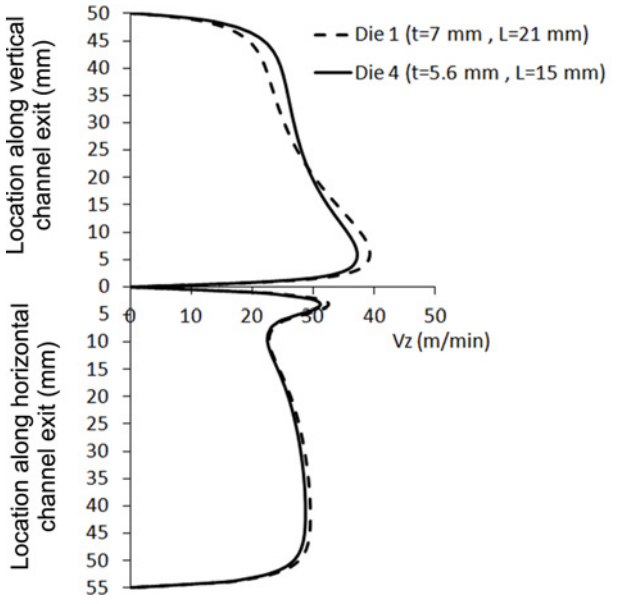

Figure 8. Velocity profiles along the center lines of the vertical channel exit plane (ES2 and ES3) and horizontal channel exit plane (ES1 and ES3).

plane is more homogeneous for the Die 4. Accordingly, optimum point is to be located around (t=5.6 mm, L=15 mm). In this case, we need to seek an alternative OF definition.

It seems that the coefficient of v_3 in f_{obj_2} should be increased for the new statement. Third OF (f_{obj_3}) is given below.

$$f_{obj\_3} = \sqrt{\frac{1}{3}[(v_1 - v_{ave})^2 + (v_2 - v_{ave})^2 + (v_3 - v_{ave})^2]} \quad (7)$$

Additionally, the results of another objective (equation (8)) function which is frequently used for flow balance problems in profile extrusion die [8,20] are shown comparatively.

$$f_{obj\_4} = \sum_{i=1}^{n} (v_i - v_{ave})^2 \quad (8)$$

Here, v_i is the polymer velocity at ith cell, v_{ave} is the average velocity and n is the number of cells at the die exit plane in 3D mesh used in numerical simulations [20]. A perfect (theoretical) balanced die having a uniform velocity at the exit leads to a measure of the die balancing equal to

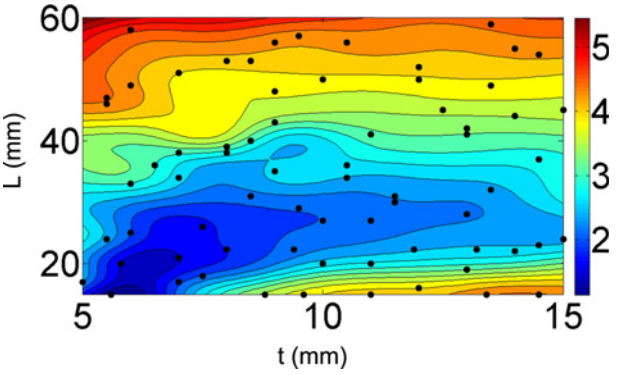

Figure 9. The contours of the objective function (f_{obj_3}) calculated by Kriging model (black points are LHS points).

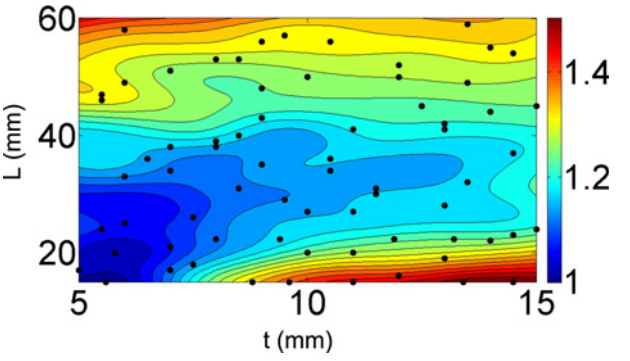

Figure 10. The contours of the objective function (f_{obj_4}) calculated by Kriging model (black points are LHS points).

Table 5. The values of objective functions (f_{obj_3}) and (f_{obj_4})

	t (mm)	L (mm)	f_{obj_3} (m/min)	f_{obj_4} (-)
Die 0	(no modification)		7.26	1.94
Die 1	7	21	1.61	1.08
Die 4	5.6	15	1.21	1.00

zero. The contours of OFs (f_{obj_3}) and (f_{obj_4}) are given in Figure 9 and 10, respectively. Since the minimum of f_{obj_4} values corresponding to 70 LHS design points is 9.93074× 10^{-6} m^2/s^2, all f_{obj_4} values are divided by the minimum f_{obj_4} value for the normalization in order to obtain f_{obj_4} values comparable to those of f_{obj_1}, f_{obj_2} and f_{obj_3}. The OF values (f_{obj_3} and f_{obj_4}) for the design points which are red-circled in Figure 7 are given in Table 5. It is seen that these two OFs are good choices for examination of flow balance for the die under investigation. However, the design point (t=5 mm, L=15 mm) at the left-bottom corner of the t-L parameter space of f_{obj_4} in Figure 10 is inside the optimum region. It is clear that in order to obtain balanced flow at the die exit the resistance of the horizontal channel is to be decreased increasing the thickness t of the thick channel. In any case, t

Table 6. The average velocities at each ES and values of objective function (f_{obj_3}) and (f_{obj_4})

	t (mm)	L (mm)	v_1 (m/min)	v_2 (m/min)	v_3 (m/min)	f_{obj_3} (m/min)	f_{obj_4} (-)
Die 0	(no modification)		9.92	27.61	19.86	7.26	1.94
Die 4	5.6	15	19.10	20.55	21.81	1.21	1.00
Die 5	5.0	15	17.18	22.05	21.08	2.10	1.03

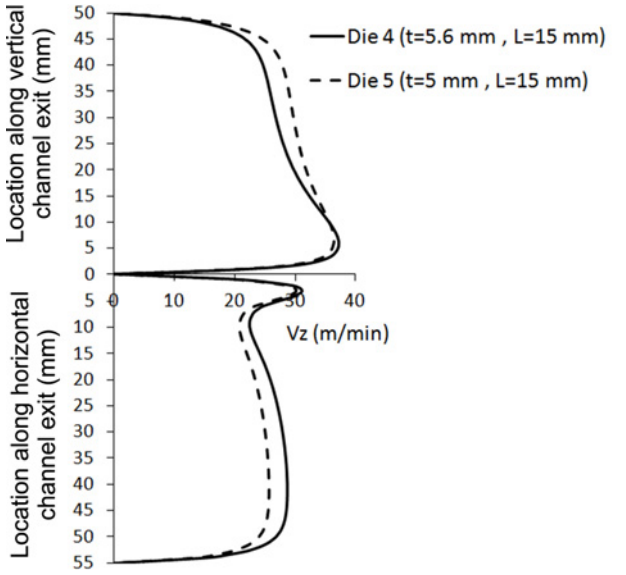

Figure 11. Velocity profiles along the center lines of the vertical channel exit plane and horizontal channel exit plane for the Die 4 and Die 5.

should be greater than the thickness of the vertical channel which is 5 mm. Hence, the design point (t=5 mm, L=15 mm) is examined in detail here. The mean velocities at each ES and values of OFs (f_{obj_3}, f_{obj_4}) for the Die 4 (t=5.6 mm, L=15 mm) and Die 5 (t=5 mm, L=15 mm) are given in Table 6. Velocity profiles along the center lines of the vertical channel exit plane and horizontal channel exit plane for the Die 4 and Die 5 in Table 6 are depicted in Figure 11. Die 4 has the lowest OF value among 70 LHS design points both for f_{obj_3} and f_{obj_4}. However, as stated above f_{obj_4} points out a performance close to that of the optimum value for the Die 5 in Figure 10 ($f_{obj\_4\_opt}$=1.00 and f_{obj_4} *(Die5)*=1.03). For the Die 5 (t=5 mm, L=15 mm) the difference between average velocities at ES1 and ES2 is nearly 5 m/min as can be seen in Table 6. This difference can also be realized by observing the velocity profiles in Figure 11.

The values of introduced 4 OFs for the investigated 5 dies are given in Table 7. In the light of results of this section, it is concluded that f_{obj_3} is the best indicator for flow balancing for the die under investigation. Hence, f_{obj_3} is used in the current optimization process. It can be concluded for the optimization of multiple-thickness profile extrusion dies that including mean velocities at intersection regions with equal constants in objective functions as separate terms will compensate unbalanced flow efficiently, because divergence of mean velocity at intersection region (ES3 in this study) from average velocity affects velocity profiles in main parts (ES1 and ES2 in this study) of the profile significantly.

Table 7. The values of objective functions for the Dies 0, 1, 2, 3, 4 and 5

	t (mm)	L (mm)	f_{obj_1} (m/min)	f_{obj_2} (m/min)	f_{obj_3} (m/min)	f_{obj_4} (-)
Die 0	(no modification)		8.93	8.58	7.26	1.94
Die 1	7	21	0.37	0.65	1.61	1.08
Die 2	11.9	22	0.30	0.94	2.55	1.24
Die 3	14.5	23	0.19	0.91	2.57	1.24
Die 4	5.6	15	0.75	0.80	1.21	1.00
Die 5	5.0	15	2.47	2.37	2.10	1.03

Optimum Die

The Simulated Annealing Kriging-Meta Algorithm is employed for the optimization of the profile die under investigation. The initial design point is (t=14 mm, L=55 mm) for the optimization process as seen in Figure 12. The following optimization algorithm parameters in Figure 3 are applied: cooling parameter c=2, initial temperature T_0=1 K and maximum iteration number k_{max}=500. Iteration number is also an affecting parameter on the optimization process. Small iteration numbers result in cessation of the optimization early without reaching the real optimum solution, whereas large iteration numbers unnecessarily lengthen the optimization process. Optimum maximum iteration number k_{max} was determined as 500 running the code repeatedly. At the end of the optimization, the global optimum design point is (t= 5.9 mm, L=15 mm) by use of f_{obj_3} and the optimum OF value is 1.15 for Kriging Interpolation and 1.21 for CFD. The optimization algorithm moves randomly from one design point to other design point in t-L parameter space during optimization process, as trial design points appear in Figure 12. Initially, optimization algorithm searches the design parameter space fast. Towards the end of the optimization process it refines the optimum found. The details of the optimization algorithm are given in our previous study [20]. The variation of current optimum f_{obj_3} during optimization process with iteration number is given in Figure 13. Optimization process reached converged solution at k=391 iterations.

The global optimum design points for all introduced OFs

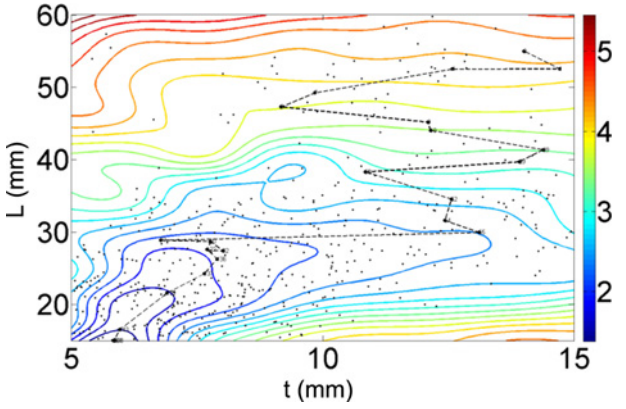

Figure 12. Optimization process of the L-shaped die based on the flow balance parameter f_{obj_3} (tiny dots: trial design points, dashed line: the solution path).

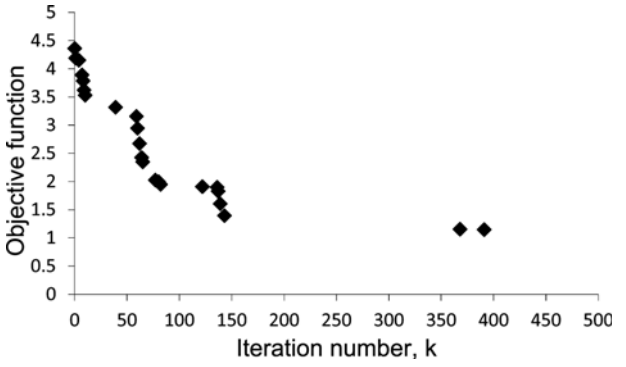

Figure 13. Variation of f_{obj_3} with iteration number.

Table 8. Optimum design points for all the introduced OFs and minimum and maximum velocity values at the exit plane of the corresponding optimum die geometries

	t_{opt} (mm)	L_{opt} (mm)	v_{min} (m/s)	v_{max} (m/s)
f_{obj_1}	14.3	23.5	0.28	0.70
f_{obj_2}	6.1	15	0.35	0.63
f_{obj_3}	5.9	15	0.38	0.62
f_{obj_4}	5.5	15	0.37	0.62

are given in Table 8. Velocity contours at the exit planes of the optimum profile dies for the introduced OFs are shown in Figures 14(b), 14(c), 14(d) and 14(e). While optimum die of f_{obj_1} is of the worst velocity distribution at the die exit plane, optimum die of f_{obj_3} is of the best uniform velocity distribution at the exit of the die under investigation. Though, optimum die geometries of f_{obj_2} and f_{obj_4} perform close to that of f_{obj_3} in terms of flow balance. However, f_{obj_3} is the best indicator for flow balance through t-L parameter space as it is shown in previous section. The difference between maximum and minimum velocities at the exit planes of the optimum dies of the introduced OFs are given

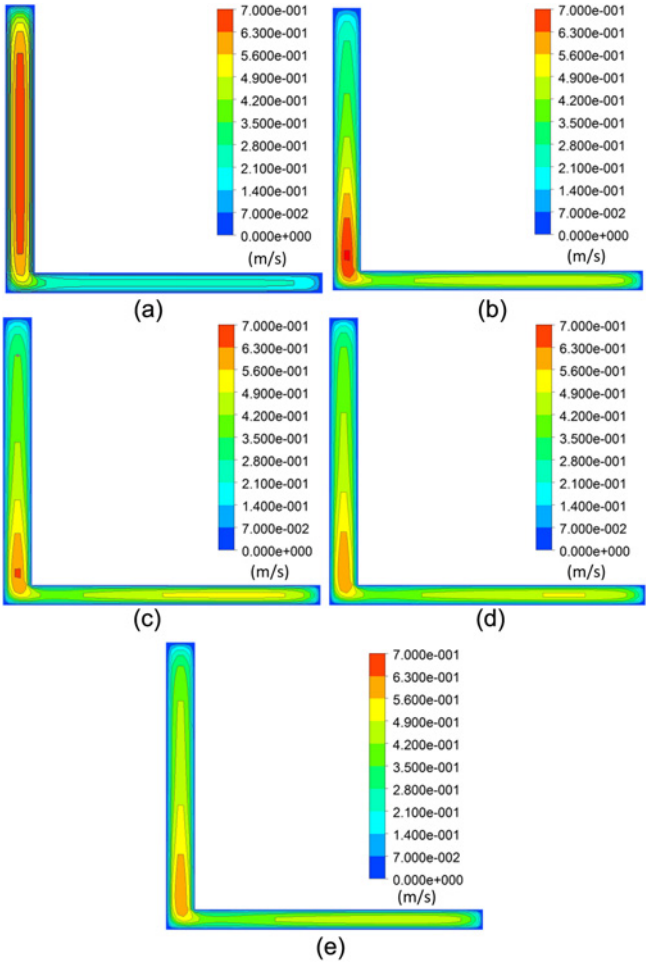

Figure 14. The velocity distribution at the exit of (a) the non-optimized die, (b) the optimum die of f_{obj_1}, (c) the optimum die of f_{obj_2}, (d) the optimum die of f_{obj_3}, and (e) the optimum die of f_{obj_4} in Table 8.

in Table 8. This difference is 0.24 m/s for the optimum die of f_{obj_3} and 0.42 m/s for the optimum die of f_{obj_1}. As flow distribution at the die exit is more balanced, difference between maximum and minimum velocities is smaller.

Velocity values in ES3 are always larger than those of the other sections ES1 and ES2 of the die exit plane, even for the best optimum die in Figure 14(d). Since the contact surface of the polymer melt with the die walls is minimum, the resistance of this section (ES3) is minimum compared to those of ES1 and ES2. On the other hand, resistance of the narrow channel which feeds ES1 enforces fluid particles to flow through channels which feed ES2 and ES3, as can be seen by observing streamlines through the optimum die geometry in Figure 15. This phenomenon is called crossflow which can be eliminated by use flow separators inside flow channels that divide flow in streams. However, use of flow separators may cause mechanical strength weakness in final products. The weighting of the mean velocity (v_3) at ES3 in

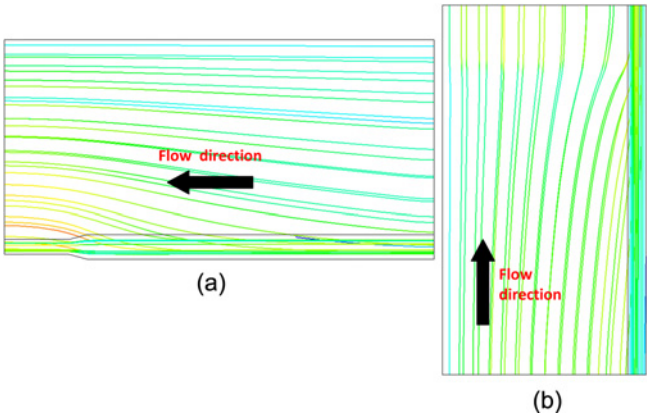

Figure 15. Stream lines through the optimum die geometry (t= 5.9 mm, L=15 mm) (a) side view and (b) top view.

equation (7) was increased from 0.33 to 0.5 and weightings of the other two terms (v_1 and v_2) in equation (7) was decreased from 0.33 to 0.25 for seeking possible better optimum design point, nevertheless the result did not change and optimum found is the same as that for f_{obj_3} which has equal weighting constants, 0.33, for three terms. The most balanced flow distribution at the die exit was achieved for the die in Figure 14(d). Velocity distribution will be regularized, while the extrudate moves ahead at ambient during production in practice.

Conclusion

In this study, the performance of 4 objective functions (OFs) is examined in terms of velocity distribution at the die exit. The results showed that the third and fourth OFs are the right choices for finding optimum die geometry for flow balance. But, the third OF is the best indicator for uniformity of velocity distribution at the exit of the die under investigation. For the optimization of multiple-thickness profile extrusion dies, it can be interpreted that incorporating average velocities at intersection regions into the objective function as separate terms with equal constants balances non-uniform velocity distribution efficiently. Difference between minimum and maximum velocities at the die exit plane is an alternative indicant for evaluation of die performance in terms of flow balance. As this difference decreases, uniformity of velocity distribution gets better. At the end of the optimization process based on f_{obj_3}, t=5.9 mm and L=15 mm at the optimum design point for the L shaped profile die in the present study.

Simulated Annealing-Kriging meta-algorithm has many advantages. First of all, the map (contours) of the OFs is produced by Kriging and the effects of die design variables on flow balancing can be clearly seen from this map. When appropriate coefficients are chosen, the Simulated Annealing Optimization Method searches the design parameter space (t-L in this study) throughly without trapping at local minimum point and finds the global optimum point. The optimization algorithm does not need an analytically defined OF. In addition, the procedure is very fast and effective. Increase in capacity and speeds of computers can make this approach efficient when used in conjuction with CFD simulations. The methodology introduced in this study can be extended to the optimization of multiple design variables.

Acknowledgement

This study is partially supported by Ministry of Science, Industry and Technology of the Turkish Republic and Mir R&D Ltd. Co. through grant number: 00309.STZ.2008-2. The authors would like to acknowledge the sponsors.

References

1. P. Hurez and P. A. Tanguy, *Polym. Eng. Sci.,* **36**, 626 (1996).
2. O. S. Carneiro, J. M. Nobrega, F. T. Pinho, and P. J. Oliveira, *J. Mater. Process. Tech.,* **114**, 75 (2001).
3. S. Kaul and W. Michaeli, *SPE ANTEC Tech. Papers,* **1**, 1 (2002).
4. J. M. Nobrega, O. S. Carneiro, P. J. Oliveira, and F. T. Pinho, *Int. Polym. Proc.*, **18**, 298 (2003).
5. O. S. Carneiro, J. M. Nobrega, P. J. Oliveira, and F. T. Pinho, *Int. Polym. Proc.*, **18**, 307 (2003).
6. J. M. Nobrega, O. S. Carneiro, F. T. Pinho, and P. J. Oliveira, *Int. Polym. Proc.*, **19**, 225 (2004).
7. O. S. Carneiro and J. M. Nobrega, *Plast. Rubber. Compos.*, **33**, 400 (2004).
8. Y. Sun and M. Gupta, *SPE ANTEC Tech. Papers*, **1**, 3307 (2004).
9. A. Zolfaghari, A. H. Behravesh, E. Shakouri, and E. Soury, *Polym. Eng. Sci*., **49**, 1793 (2009).
10. A. Zolfaghari, A. H. Behravesh, E. Shakouri, and E. Soury, *Polym. Eng. Sci.*, **50**, 543 (2010).
11. A. R. Shahreza, A. H. Behravesh, M. B. Jooybari, and E. Soury, *Polym. Eng. Sci.*, **50**, 2417 (2010).
12. I. Szarvasy, J. Sienz, J. F. T. Pittman, and E. Hinton, *Int. Polym. Proc.*, **15**, 28 (2000).
13. H. J. Ettinger, J. Sienz, J. F. T. Pittman, and A. Polynkin, *Struct. Multidiscip. O.*, **28**, 180 (2004).
14. J. Švábík, L. Placek, and P. Sáha, *Int. Polym. Proc.*, **14**, 247 (1999).
15. Y. Dai, H. Zheng, C. Zhou, and W. Yu, *J. Macromol. Sci. Pure,* **45**, 1028 (2008).
16. W. Michaeli, "Extrusion Dies for Plastics and Rubber: Design and Engineering Computations", 3rd ed., pp.207-222, Hanser, Münich, 2003.
17. B. L. Koziey, J. Vlachopoulos, J. Vlek, and J. Svabik, *SPE ANTEC Tech. Papers*, **1**, 247 (1996).
18. P. Hurez and P. A. Tanguy, *Polym. Eng. Sci.*, **33**, 971 (1993).

19. J. F. T. Pittman, *P. I. Mech. Eng. E.-J. Pro.*, **225**, 280 (2011).
20. O. Yilmaz, H. Gunes, and K. Kirkkopru, "Design Optimization of an L-Shaped Extrusion Die", Vol.9, p.147, ASME International Mechanical Engineering Congress & Exposition IMECE2009, Florida, ABD, 13-19 November, 2009.
21. M. D. McKay, W. J. Conover, and R. J. Beckman, *Technometrics*, **21**, 239 (1979).
22. H. E. Cekli, "Enhancement and Smoothing Methods for Experimental Data: Application to PIV Measurements of a Laminar Separation Bubble", Ph. D. Dissertation, Istanbul Tech. Uni., Istanbul, 2007.
23. PolyFlow, http://www.ansys.com.
24. D. G. Krige, *J. Chem. Metal. Mining Soc. South Africa*, **52**, 119 (1951).
25. G. Matheron, "Traite de Geostatistique Appliquee", 1st ed., pp.334-350, Paris, Editions Technip, 1962.
26. S. Kirkpatrick, C. D. Gelatt, and M. P. Vecchi, *Science*, **220**, 671 (1983).
27. D. G. Baird and D. I. Collias, "Polymer Processing: Principles and Design", 1st ed., pp.20-23, New York, Wiley-Interscience Publication, 1998.
28. R. B. Bird, R. C. Armstrong, and O. Hassager, "Dynamics of Polymeric Liquids", 2nd ed., Vol. 1, p.105, New York, Wiley-Interscience publication, 1987.